East European Journal of Physics. 3. 505-511 (2025)
DOI:10.26565/2312-4334-2025-3-56 ISSN 2312-4334

# INFLUENCE OF RADIO-FREQUENCY MAGNETRON SPUTTERING PARAMETERS ON THE STRUCTURE AND PERFORMANCE OF Al AND $Al_2O_3$ THIN FILMS

**R. Ramos Blazquez[a]*, F. Solís-Pomar[a]*, A. Fundora[b], M.A. Ruiz-Robles[a], Amilkar Fragiel[c], Eduardo Pérez-Tijerina[a]**

[a]*Universidad Autónoma de Nuevo León, Centro de Investigación en Ciencias Físico Matemáticas, Facultad de Ciencias Físico-Matemáticas, Av. Universidad S/N. Ciudad Universitaria, 66451, San Nicolás de los Garza, Nuevo León, México*
[b]*Instituto Superior de Tecnologías y Ciencias Aplicadas, Universidad de la Habana, Ave. Salvador Allende Nº 1110 CP 10400, La Habana, Cuba*
[c]*Centro de Física, Instituto Venezolano de Investigaciones Científicas – IVIC, Apartado 20632, Caracas 1020-A, Venezuela*
**Corresponding Authors E-mail: francisco.solispm@uanl.edu.mx; rramos9708@gmail.com**
Received June 13, 2025; revised August 22, 2025; accepted August 28, 2025

In this work, the structural, morphological and optical properties of aluminum (Al) and aluminum oxide ($Al_2O_3$) thin films deposited by radio-frequency (RF) magnetron sputtering were studied. The films were grown using a high–purity Al target in controlled atmospheres containing varying flows of argon (Ar) and oxygen ($O_2$). Particular attention was given to how the target-substrate distance and the Ar/$O_2$ flow ratios influence the films' structural properties, surface features, and optical response. Characterization techniques included X-ray diffraction (XRD) for phase identification and crystallite size estimation, Atomic Force Microscopy (AFM) for surface morphology and roughness analysis, and UV–Vis Spectroscopy for optical transmittance measurements. The results showed that reducing the target-substrate distance led to films with increased surface roughness, thickness, grain size and crystallite size, likely due to enhanced energetic bombardment and adatom mobility. Optical measurements revealed that $Al_2O_3$ films grown at higher $O_2$ flow rates (around 5 sccm) were highly transparent, exhibiting transmittance values close to 100% across the UV-visible range (190-900 nm). In contrast, films deposited under low $O_2$ flow conditions (0.6-1.4 sccm) were nearly opaque, indicating incomplete oxidation or metallic behavior. The XRD analysis revealed that higher $O_2$ flows tended to suppress crystallinity, resulting in amorphous $Al_2O_3$ films, while lower flows preserved some degree of crystalline order. Additionally, increasing the Ar flow rate during deposition promoted films growth, as evidenced by increased film thickness, which may be attributed to enhanced sputtering efficiency and target atom flux. These findings highlight the critical role of deposition parameters in tailoring the properties of Al-based thin films for optical and electronic applications.
**Keywords:** *Aluminum; Thin films; Magnetron sputtering; Target-substrate distance; Ar flow rate*
**PACS:** 81.15.Cd, 68.37.Ps, 61.05.cp, 78.66.Bz

## INTRODUCTION

In recent years, thin film technology has emerged as a significant research area worldwide, driving the development of innovative techniques for film growth [1]. The structural properties of thin films depend on their synthesis method, with a preference in the literature for physical methods, primarily thermal and vapor deposition [1]. Physical deposition methods produce films with higher adhesion and require lower substrate temperatures. In contrast, the main drawback of chemical methods is their reliance on toxic solvents [2]. The properties of the resulting films depend on the deposition conditions used; in sputtering, these conditions include power [3,4,5], deposition time [6,7], working pressure, gases used [8-10], substrate temperature [11,3], target-substrate distance [12, 13], and other factors.

Metallic coatings are versatile and suitable for a diverse range of applications. Pure metals such as aluminum, nickel, tungsten, and titanium are commonly used in optical and energy applications [14,15].

$Al_2O_3$ films are frequently applied in various fields, including optics [8], cutting tool applications [16], and as insulating layers in gate dielectric components [17]. Due to their low refractive index and high optical transparency, alumina films are often utilized as anti-reflective coatings in solar cells [18].

In solar-to-thermal conversion, the selective solar absorber plays a crucial role by efficiently absorbing solar radiation over a broad wavelength range while minimizing infrared re-radiation as the absorber's temperature increases [19–21]. To enhance the thermal stability of selective solar absorber multilayers, $Al_2O_3$ layers have been used in [22] via atomic layer deposition (ALD) to suppress metal atom diffusion from the underlying reflective layer.

$Al_2O_3$ also has significant potential as a coating in thermonuclear fusion applications due to its high permeation reduction factor (PRF), good irradiation resistance, compatibility with Pb-Li, and strong corrosion resistance, mechanical durability, and wear resistance [23, 24].

Magnetron sputtering technology enables the deposition of thin films over large areas with high deposition rates and good adhesion, making it a preferred method for producing thin-film metallic coatings with less environmental impact than chemical methods [25].

To optimize the application of these films and coatings, it is essential to understand how deposition conditions affect their properties. The impact of sputtering power on film properties has been widely studied [1,4,5]. In this article, we

***Cite as***: R.R. Blazquez, F. Solís-Pomar, A. Fundora, M.A. Ruiz-Robles, A. Fragiel, E.P. Tijerina, East Eur. J. Phys. 3, 505 (2025), https://doi.org/10.26565/2312-4334-2025-3-56

investigate the relationship between target-substrate distance, Ar and $O_2$ flow rates, and the resulting morphological, crystallographic, and optical properties of the films.

## METHODOLOGY

### Thin film synthesis

The films were deposited onto glass substrates by magnetron sputtering using a 13.56 MHz radio-frequency (RF) source with an Al target in an environment of high-purity Ar (99.999%) and $O_2$. The Al target, 99.99% pure, measured 2 inches in diameter and 0.25 inches in thickness and was cleaned by pre-sputtering for 40 minutes. The substrate surfaces were treated with Ar before deposition. A base pressure of $3.5 \times 10^{-5}$ Torr was achieved using a mechanical pump and a turbomolecular pump.

For the characterization of the films by X-ray diffraction (XRD), an X'Pert³ Powder diffractometer was used at 45 kV and 40 mA with a wavelength of $\lambda = 1.5406$ Å. Data processing was performed using the X'Pert HighScore Plus software, and the patterns were indexed with assistance from the International Center for Diffraction Data (ICDD) database. Crystallite size calculations were performed using the Scherrer equation.

Atomic force microscopy (AFM) results were obtained with a Park Systems Corp. NX10 microscope in non-contact mode, equipped with an $SiO_2$ tip. Optical characterization was performed using a Jasco V-750 UV-Vis spectrophotometer over a wavelength range of 190-900 nm.

**Table 1** presents the deposition conditions used for Al and $Al_2O_3$ thin films, illustrating the various parameters employed to investigate the effects of target-substrate distance, as well as argon and oxygen flow rates.

**Table 1.** Deposition parameters for Al and $Al_2O_3$ thin films synthesized by RF magnetron sputtering.

| Deposition Parameter | Al films (Target-substrate distance study) | Al films (Ar flow study) | $Al_2O_3$ films ($O_2$ flow study) |
|---|---|---|---|
| Target-substrate distance (cm) | 6, 9, 12 | 9 | 9 |
| Argon Flow rate (sccm) | 40 | 20, 40, 60 | 50 |
| Oxygen Flow rate (sccm) | | | 0.6, 1.0, 1.4, 5.0 |
| Working pressure (mTorr) | 5.0 | 3.5, 5.0, 7.0 | 5.0, 5.1, 5.2, 5.5 |
| Deposition time (min) | 15 | 15 | 30 |
| Power (W) | 150 | 150 | 270 |

## RESULTS AND DISCUSSION

### Al thin film grown at different target-substrate distances

The AFM technique enabled us to characterize the surface and thickness of the films. **Figure 1** displays the 2D AFM images of the films, while **Figure 2** illustrates the dependence of roughness and thickness on the target-substrate distance.

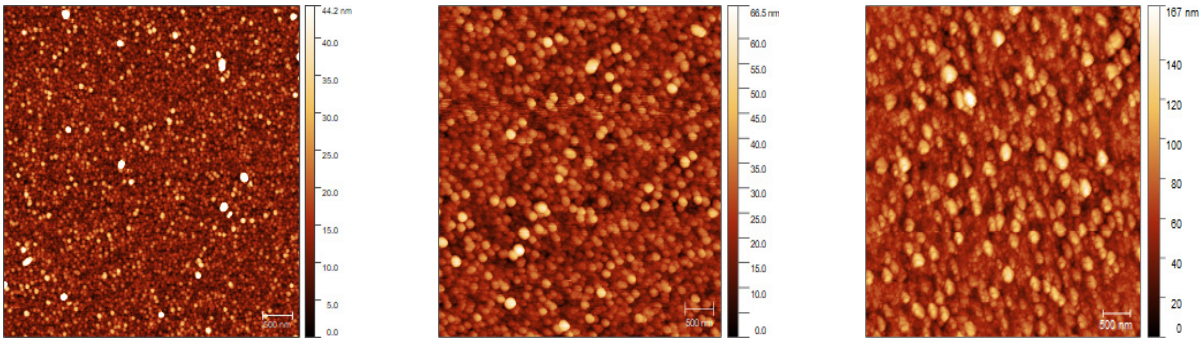


**Figure 1.** 2D AFM images of films grown (from left to right) at: 12, 9 and 6 cm target-substrate distance, the root mean square roughness turned out to be: 6.3, 8.0 and 20.4 nm, respectively

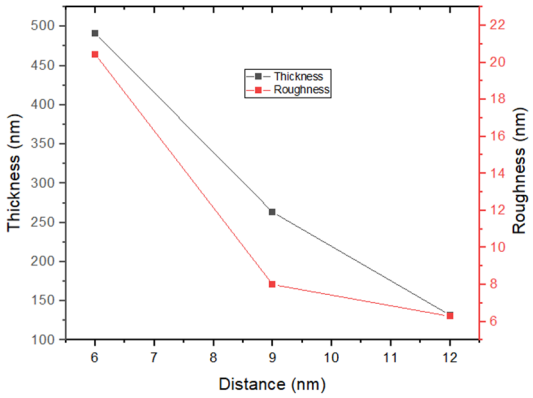


**Figure 2.** Decrease in the thickness and roughness of the films by increasing the target-substrate distance.

As shown in Figures 1 and 2, roughness, grain size, and thickness decrease as the target-substrate distance increases **(Table 2)**. With a greater target-substrate distance, the eroded atoms travel farther before deposition, resulting in an increased number of collisions along their trajectory. This reduces both the kinetic energy with which they reach the substrate or growing film and the number of atoms that complete the entire path to deposition [26, 27].

Statistical analysis was conducted to quantify the increase in grain size, using the software XEI from Park Systems.

**Table 2.** Summary of AFM results for film characterization

| Target-substrate distance (cm) | 6 | 9 | 12 |
|---|---|---|---|
| Thickness (nm) | 491 | 263 | 132 |
| Deposition rate (nm/min) | 32.7 | 17.5 | 8.8 |
| Root mean square roughness (nm) | 20.4 | 8.0 | 6.3 |
| Average grain length (nm) | 155 | 125 | 90 |
| Average grain perimeter (nm) | 468 | 390 | 271 |

The diffraction patterns of the films grown at different target-substrate distances were analyzed. Using X'Pert HighScore Plus software and the Scherrer equation, the crystallite size was calculated for each family of planes present in the pattern.

**Figure 3** shows the obtained diffraction patterns. These correspond to a cubic system with space group Fm-3m. As shown in the graph, decreasing the target-substrate distance results in higher peak intensities, which reflects an improved signal-to-noise ratio. This makes the fluctuations less noticeable, giving the diffraction lines a clearer and sharper appearance. This effect can be attributed to a higher deposition rate and larger crystallite formation at shorter distances. The increased kinetic energy of aluminum atoms enhances their mobility on the surface and along grain boundaries, promoting grain coalescence and growth [27].

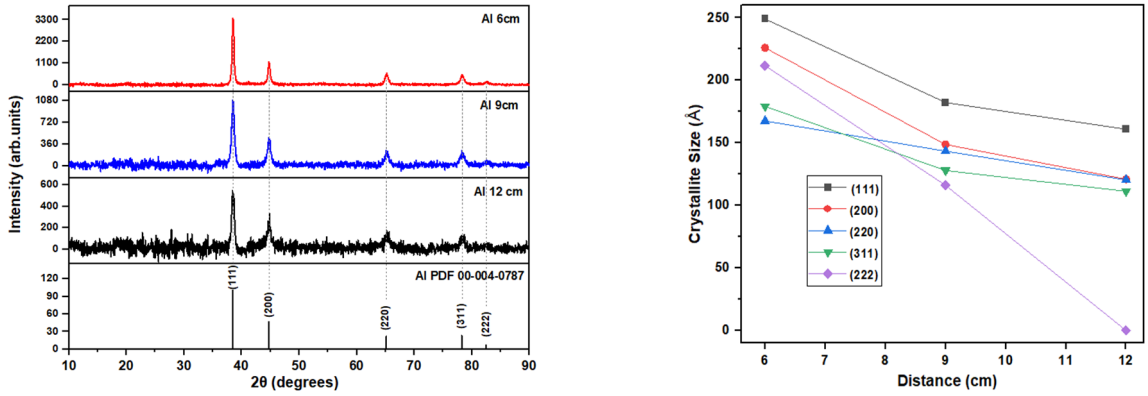


**Figure 3.** XRD patterns and decrease in crystallite size with the increasing in target-substrate distance for Al thin films

## Al thin films grown at different Ar flow rates

**Figure 4** shows the 2D AFM images obtained for these films, along with the root mean square roughness. The roughest film, as well as the one with the largest grain size, was obtained with 40 sccm of Ar **(Table 3)**.

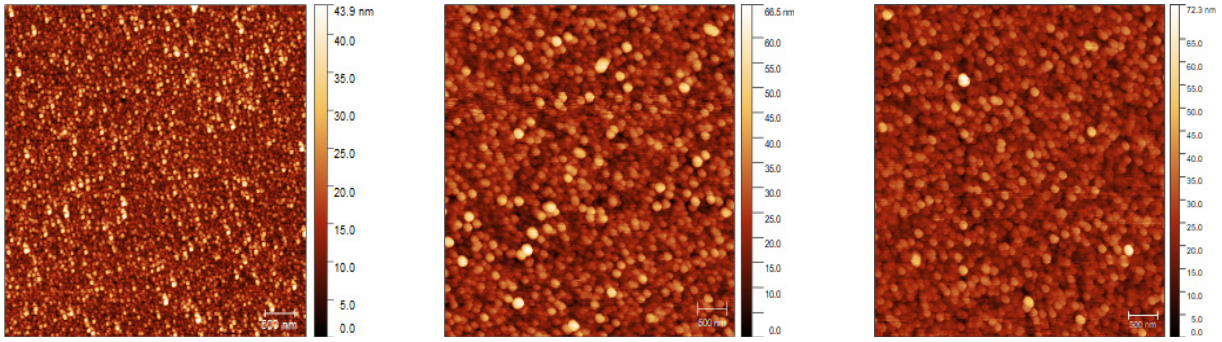

**Figure 4.** 2D AFM images of films grown (from left to right) at: 20, 40 and 60 sccm of Ar flow rate, the root mean square roughness was found to be: 5.8, 8.0 and 6.6 nm, respectively

**Figure 5** shows an increase in thickness with the Ar flow rate. As the argon flow rate increases, a greater number of atoms are sputtered from the target, generally leading to an increase in thickness. However, when the argon flow becomes too high, the mean free path of the sputtered particles is reduced due to more frequent collisions, which can limit their ability to reach the substrate and consequently reduce the films thickness [28, 29]. Therefore, the thickness of the Al films is a competition of the above-mentioned effects. A decrease in roughness for the film grown at 60 sccm is also observed

in Figure 5. Similar behavior was reported by Chavan et al [28] in RF-sputtered Mo thin films. At 60 sccm, the higher flow reduces adatom energy and surface mobility, which limits the formation of large islands and promotes more uniform layer-by-layer growth, resulting in smoother films and lower roughness compared to 40 sccm, were higher mobility favors larger grains and a rougher surface.

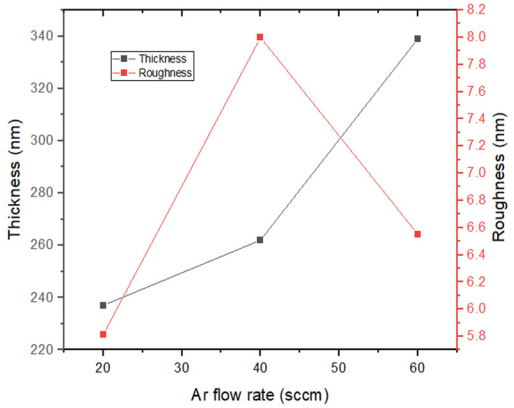


**Figure 5.** Behavior of the thickness and roughness of the films grown at different Ar fluxes.

**Table 3.** Summary of AFM results for film characterization.

| Ar flow rate (sccm) | 20 | 40 | 60 |
|---|---|---|---|
| Thickness (nm) | 237 | 263 | 339 |
| Deposition rate (nm/min) | 15.8 | 17.5 | 22.6 |
| Root mean square roughness (nm) | 5.8 | 8.0 | 6.6 |
| Average grain length (nm) | 102 | 125 | 119 |
| Average grain perimeter (nm) | 282 | 390 | 377 |

**Figure 6** shows the diffraction patterns obtained. The film synthesized at 40 sccm of Ar exhibits a larger grain size, which translates into an improvement in crystalline properties, such as crystallite size (Figure 8). An analogous behavior in crystallite size was observed by Akhtaruzzaman et al. [30] in their study of $WS_2$ films deposited at different argon flow rates. The XRD peak intensities are governed by a combination of factors [31]. At low Ar flow (20 sccm), smoother surfaces and higher adatom mobility enhance coherent diffraction, producing the highest intensities. At 40 sccm, larger crystallites and good texture maintain relatively high peaks despite higher roughness, while at 60 sccm, defects and reduced mobility lower the peak intensities even for thicker films.

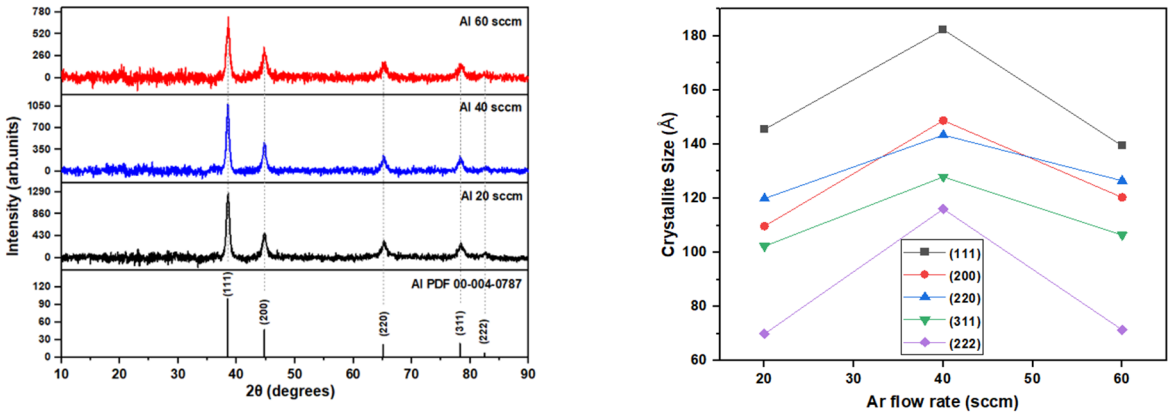


**Figure 6.** XRD patterns of Al samples grown at different Ar fluxes

### $Al_2O_3$ thin films grown at different $O_2$ flow rates

The crystalline properties of $Al_2O_3$ films grown with an Al target in an Ar and $O_2$ environment, at different $O_2$ flow rates, were studied. Table 1 shows the deposition parameters used.

**Figure 7** shows the obtained diffraction patterns, where we can observe a considerable decrease in crystalline properties as the amount of oxygen increases. The structural evolution of the films with oxygen flow can be described as follows: the samples grown at 0.6 and 1.0 sccm exhibit clear diffraction peaks corresponding to metallic Al, indicating that these films are crystalline. The sample deposited at 1.4 sccm shows weaker and broader peaks, consistent with a significant reduction in crystallite size and amorphization due to the incorporation of oxygen. Finally, the film grown at 5.0 sccm exhibits no discernible diffraction peaks, indicating a fully amorphous structure. In addition, a slight angular

shift of the diffraction peaks was observed, which can be attributed to changes in the lattice parameters. This progressive loss of crystallinity and peak displacement are expected, as oxygen incorporation disrupts the ordered arrangement of Al atoms in the metallic lattice and promotes the formation of an amorphous Al-O network. [32, 33].

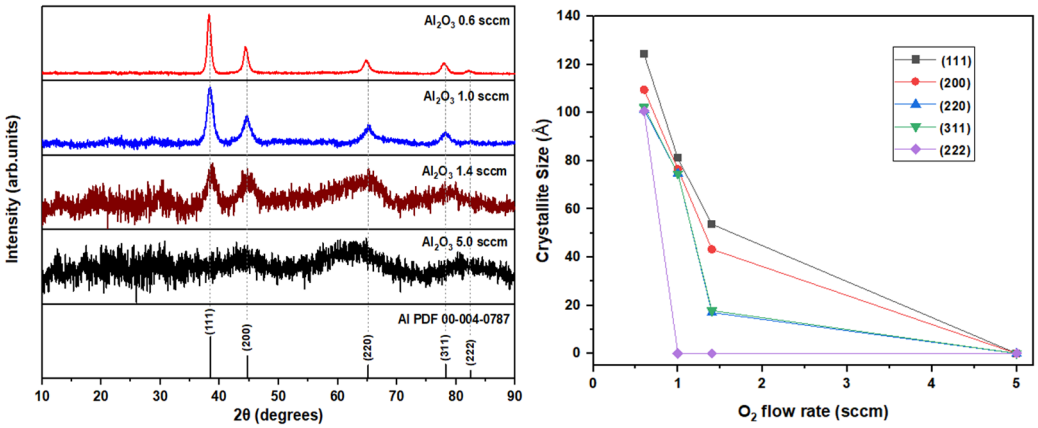


**Figure 7.** XRD patterns of $Al_2O_3$ samples grown at different $O_2$ flow rates. Decrease in crystallite size with increasing $O_2$ flow rate.

The optical properties of these films strongly depend on the $O_2$ flow rate. In **Figure 8**, we can observe that the film grown at the highest oxygen flow rate (5 sccm) has a transmittance of almost 100%, while the films synthesized at 0.6, 1.0, and 1.4 sccm have almost 0% transmittance across the range 290-900 nm and decreasing from ≈8% to nearly 0% in the 190-290 nm range. These values reflect the strong absorption of the films. The spectral shape is further modulated by the onset of absorption in the glass substrate, which produces small oscillations in this range. Such oscillations are also visible for the 5 sccm sample despite its high transparency.

The depression in transmittance near 300 nm for the film grown at 5 sccm is consistent with interference in the near-UV and is mainly attributed to thin-film optical interference (film/substrate coupling). This interpretation is supported by the calculation of an interference minimum at 300 nm for a film thickness of 132.4 nm, which closely matches the experimental thickness of our film (133.8 nm).

The thickness of the samples was measured using the height difference between the film and the substrate in AFM. As shown in **Figure 9,** the film thickness decreases as the $O_2$ flow rate increases. At low $O_2$ flows, the aluminum target remains largely metallic, allowing a high sputtering yield and resulting in thicker films. As the $O_2$ flow increases, a layer of aluminum oxide forms on the target surface, which has a much lower sputtering yield compared to metallic Al. Although RF sputtering allows stable plasma operation even when the target becomes partially insulating, the deposition rate still decreases significantly because the sputtering efficiency of the oxidized target is lower. This process is known as poisoned target effect in reactive sputtering [34]. Consequently, films deposited under higher $O_2$ flow are thinner.

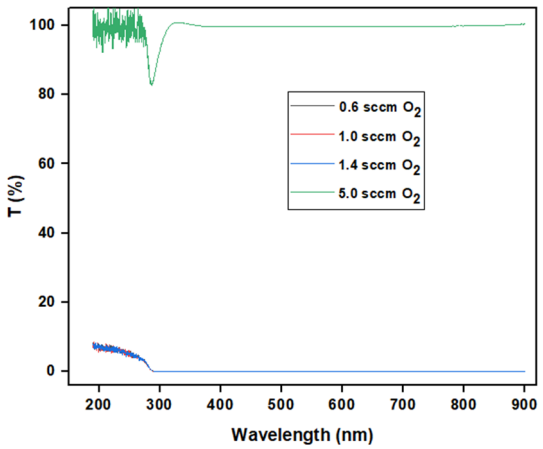


**Figure 8.** Transmittance of $Al_2O_3$ films grown at different $O_2$ flow rates

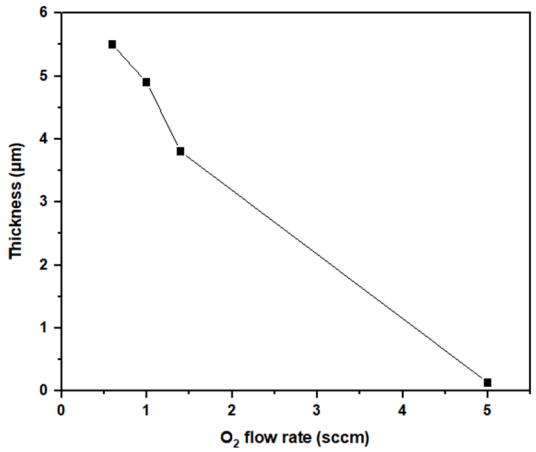


**Figure 9.** Behavior of the thickness of the $Al_2O_3$ films grown at different $O_2$ fluxes

## CONCLUSIONS

In this work, Al and $Al_2O_3$ films were deposited by magnetron sputtering with a radio-frequency source. For the Al films, we used an Ar environment, while for the $Al_2O_3$ films, a mixture of Ar and $O_2$ was used. In the first case, we studied the influence of the target-substrate distance (6, 9, 12 cm) on the morphological and crystallographic properties of the films. AFM analysis revealed an increase in roughness, thickness, and grain size as the target-substrate distance decreased. XRD results showed that the crystalline properties of the samples improved as the target was brought closer to the

substrate, which is associated with the intentional increase in substrate temperature and grain fusion, contributing to the formation of a more uniform crystalline structure with fewer grain boundaries.

In the second case, we examined the influence of Ar flow rate (20, 40, 60 sccm). The film grown at 40 sccm was the roughest, with the largest grain and crystallite size. Furthermore, increasing the Ar flow rate led to an increase in film thickness.

For the $Al_2O_3$ samples, we studied the influence of $O_2$ flow rate, using a fixed Ar flow of 50 sccm while varying the $O_2$ flow (0.6, 1.0, 1.4, 5.0 sccm). We observed a significant decrease in crystalline properties as the oxygen flow increased, due to the introduction of oxygen atoms disrupting the orderly arrangement of atoms in the crystal lattice. The film grown at the highest oxygen flow exhibited a transmittance of almost 100%, while the films synthesized at 0.6, 1.0 and 1.4 sccm showed nearly 0% transmittance across the 290-900 nm range. In addition, the film thickness decreased with increasing $O_2$ flow due to the poisoning of the target during reactive sputtering.

**Acknowledgements**

R. Ramos Blazquez acknowledges CONAHCYT for his master studies scholarship (843048).

**ORCID**

**R. Ramos Blazquez,** https://orcid.org/0009-0008-6274-7640; **F. Solis-Pomar,** https://orcid.org/0000-0002-4536-6538
**A. Fundora,** https://orcid.org/0000-0001-8809-7529; **M. A. Ruiz-Robles,** https://orcid.org/0000-0003-4834-8025
**E. Pérez-Tijerina,** https://orcid.org/0000-0001-9742-4093

**REFERENCES**

[1] F.M. Mwema, O.P. Oladijo, S.A. Akinlabi, and E.T. Akinlabi, "Properties of physically deposited thin aluminium film coatings: A review," Journal of Alloys and Compounds, **747**, (2018) 306-323. https://doi.org/10.1016/j.jallcom.2018.03.006

[2] J. Tao, J. Liu, L. Chen, H. Cao, X. Meng, Y. Zhang, C. Zhang, *et al*., "7.1% efficient Co-electroplated $Cu_2ZnSnS_4$ thin film solar cells with sputtered CdS buffer layers," Green Chem. **18**(2), 550-557 (2016). https://doi.org/10.1039/C5GC02057C

[3] S. Ponmudi, R. Sivakumar, C. Sanjeeviraja, and C. Gopalakrishnan, "Infuences of sputtering power and annealing temperature on the structural and optical properties of $Al_2O_3$:CuO thin films fabricated by radio-frequency magnetron sputtering technique," Journal of Materials Science: Materials in Electronics, **30**, 18315–18327 (2019). https://doi.org/10.1007/s10854-019-02185-0

[4] M. Lee, *et. al*., "Influence of sputtering conditions on the properties of aluminum-doped zinc oxide thin film fabricated using a facing target sputtering system," Thin Solid Films, **703**, 137980 (2020). https://doi.org/10.1016/j.tsf.2020.137980

[5] S. Asgary, *et al*., "Magnetron sputtering technique for analyzing the influence of RF sputtering power on microstructural surface morphology of aluminum thin films deposited on $SiO_2$/Si substrates," Applied Physics A, **127**, 752 (2021). https://doi.org/10.1007/s00339-021-04892-0

[6] A. Tchenka, *et al*., "Effect of RF sputtering power and deposition time on optical and electrical properties of indium tin oxide thin film," Advances in Materials Science and Engineering, **2021**(1), 5556305 (2021). https://doi.org/10.1155/2021/5556305

[7] V. Karoutsos, *et al*., "On the Effect of Randomly Oriented Grain Growth on the Structure of Aluminum Thin Films Deposited via Magnetron Sputtering," Coatings, **14**, 1441 (2024). https://doi.org/10.3390/coatings14111441

[8] M. Akhtaruzzaman, M. Shahiduzzaman, N. Amin, G. Muhammad, M.A. Islam, K.S.B. Rafiq, and K. Sopian, "Impact of Ar flow rates on micro-structural properties of WS2 thin film by RF magnetron sputtering," Nanomaterials, **11**(7), 1635 (2021). https://doi.org/10.3390/nano11071635

[9] J. Wang, *et al*., "Enhanced formation of α-$Al_2O_3$ at low temperature on Cr/Al coating by controlling oxygen partial pressure," Applied Surface Science, **515**, 146053 (2020). https://doi.org/10.1016/j.apsusc.2020.146053

[10] M.K. Sandager, C. Kjelde, and V. Popok, "Growth of thin AlN films on Si wafers by reactive magnetron sputtering: Role of processing pressure, magnetron power and nitrogen/argon gas flow ratio," Crystals, **12**(10), 1379 (2022). https://doi.org/10.3390/cryst12101379

[11] Y. Gao, H. Leiste, S. Heissler, S. Ulrich, and M. Stueber, "Optical properties of radio-frequency magnetron sputtered α-$(Cr_{1-x}Al_x)_2O_3$ thin films grown on α-$Al_2O_3$ substrates at different temperatures," Thin Solid Films, **660**, 439–446 (2018). https://doi.org/10.1016/j.tsf.2018.06.053

[12] G. Zhu, Y. Yang, B. Xiao, and Z. Gan, "Evolution Mechanism of Sputtered Film Uniformity with the Erosion Groove Size: Integrated Simulation and Experiment," Molecules, **28**(22), 7660 (2023). https://doi.org/10.3390/molecules28227660

[13] Z. Wei, L. Shen, Y. Kuang, J. Wang, G. Yang, and W. Lei, „The evolution of preferred orientation and morphology of AlN films under various sputtering parameters," Journal of Crystal Growth, **625**, 127439 (2024). https://doi.org/10.1016/j.jcrysgro.2023.127439

[14] A. Baptista, *et al*., "Sputtering Physical Vapour Deposition (PVD) Coatings: A Critical Review on Process Improvement and Market Trend Demands," Coatings, **8**, 402 (2018). https://doi.org/10.3390/coatings8110402

[15] J. Cheng, *et al*., "Research on magnetron sputtering thin films as electrode materials for supercapacitors," Chemical Engineering Journal, **509**, 161242 (2025). https://doi.org/10.1016/j.cej.2025.161242

[16] M. Singh, *et. al*., "Deposition and Characterization of Aluminium Thin film Coatings using DC Magnetron Sputtering Process," Materials Today: Proceedings, **5**, 2696–2704 (2018). https://doi.org/10.1016/j.matpr.2018.01.050

[17] Y. Gao, *et al*., "The process of growing $Cr_2O_3$ thin films on α-$Al_2O_3$ substrates at low temperature by r.f. magnetron sputtering," Journal of Crystal Growth, **457**, 158-163 (2017). https://doi.org/10.1016/j.jcrysgro.2016.08.009

[18] J. Cheng Ding, *et al*., "Low-temperature deposition of nanocrystalline $Al_2O_3$ films by ion source-assisted magnetron sputtering," **149**, 284-290 (2018). https://doi.org/10.1016/j.vacuum.2018.01.009

[19] K.C. Chung, and W.-H. Lee, "Effect of pretreatment on $Al_2O_3$ substrate by depositing $Al_2O_3$ film on the properties of Ni–Cr–Si based thin film resistor," Materials Chemistry and Physics, **234**, 311–317 (2019). https://doi.org/10.1016/j.matchemphys.2019.05.058

[20] Y. Ning, *et al*., "NiCrAlO/$Al_2O_3$ solar selective coating prepared by direct current magnetron sputtering and water boiling," Solar Energy Materials and Solar Cells, **219**, 110807 (2021). https://doi.org/10.1016/j.solmat.2020.110807

[21] Y. Wu, *et al*., "Enhanced thermal stability of the metal/dielectric multilayer solar selective absorber by an atomic-layer-deposited $Al_2O_3$ barrier layer," Applied Surface Science, **541**, 148678 (2021). https://doi.org/10.1016/j.apsusc.2020.148678
[22] P. Li, *et al*., "Copper-Doped Chromium Oxide Hole-Transporting Layer for Perovskite Solar Cells: Interface Engineering and Performance Improvement," Adv. Mater. Interfaces, **3**, 1500799 (2016). https://doi.org/10.1002/admi.201500799
[23] E.B. Kashkarov, D.V. Sidelev, M. Rombaeva, M.S. Syrtanov, and G.A. Bleykher, "Chromium coatings deposited by cooled and hot target magnetron sputtering for accident tolerant nuclear fuel claddings," Surface & Coatings Technology, **389**, 125618 (2020). https://doi.org/10.1016/j.surfcoat.2020.125618
[24] S. Ozen, V. Senay, "Optical, Morphological and Nano-Mechanical Properties of Chromium Oxide Thin Films Fabricated by Radio-Frequency (RF) Magnetron Sputtering," Optik, **201**, 163433 (2020). https://doi.org/10.1016/j.ijleo.2019.163433
[25] J. Li, *et al*., "Facilitating Complex Thin Film Deposition by Using Magnetron Sputtering: A Review," JOM, **74**, 3069–3081 (2022). https://doi.org/10.1007/s11837-022-05294-0
[26] *Handbook of thin film deposition*, edited by K. Seshan, and D. Schepis, (William Andrew, 2018).
[27] J.A. Lenis, M.A. Gómez, and F.J. Bolívar, "Effect of deposition temperature and target-substrate distance on the structure, phases, mechanical and tribological properties of multi-layer HA Ag coatings obtained by RF magnetron sputtering," Surface & Coatings Technology, **378**, 124936 (2019). https://doi.org/10.1016/j.surfcoat.2019.124936
[28] P. Yi, W. Zhang, F. Bi, L. Peng, and X. Lai, "Microstructure and properties of a-C films deposited under different argon flowrate on stainless steel bipolar plates for proton exchange membrane fuel cells," Journal of Power Sources, **410-411**, 188-195 (2019). https://doi.org/10.1016/j.jpowsour.2018.10.054
[29] K.B. Chavan, S.V. Desarada, and N.B. Chaure, "Influences of substrate temperature and Ar flow on the properties of RF sputtered Mo thin films," Journal of Materials Science: Materials in Electronics, **31**(13), 10306-10314 (2020). https://doi.org/10.1007/s10854-020-03578-2
[30] Md. Akhtaruzzaman, *et al*., "Impact of Ar Flow Rates on Micro-Structural Properties of $WS_2$ Thin Film by RF Magnetron Sputtering," Nanomaterials, **11**, 1635 (2021). https://doi.org/10.3390/nano11071635
[31] H. Khan, A.S. Yerramilli, A. D'Oliveira, T.L. Alford, D.C. Boffito, and G.S. Patience, "Experimental methods in chemical engineering: X-ray diffraction spectroscopy—XRD," The Canadian journal of chemical engineering, **98**(6), 1255-1266 (2020). https://doi.org/10.1002/cjce.23747
[32] M. Sowjanya, *et al*., "Impact of Ar:$O_2$ gas flow ratios on microstructure and optical characteristics of $CeO_2$-doped ZnO thin films by magnetron sputtering," EPL, **135**, 67003 (2021). https://doi.org/10.1209/0295-5075/ac2d55
[33] G. Angarita, C. Palacio, M. Trujillo, and M. Arroyave, "Synthesis of alumina thin films using reactive magnetron sputtering method," Journal of Physics: Conference Series, **850**(1), 012022 (2017). https://doi.org/10.1088/1742-6596/850/1/012022
[34] M. Arif, and C. Eisenmenger-Sittner, „In situ assessment of target poisoning evolution in magnetron sputtering," Surface and Coatings Technology, **324**, 345-352 (2017). https://doi.org/10.1016/j.surfcoat.2017.05.047

## ВПЛИВ ПАРАМЕТРІВ РАДІОЧАСТОТНОГО МАГНЕТРОННОГО РОЗПИЛЕННЯ НА СТРУКТУРУ ТА ХАРАКТЕРИСТИКИ ТОНКИХ ПЛІВОК Al ТА $Al_2O_3$

**Р. Рамос Бласкес[a], Ф. Соліс-Помар[a], А. Фундора[b], М.А. Руїс-Роблес[a], Амілкар Фрагіель[c], Едуардо Перес-Тіхеріна[a]**
*[a]Автономний університет Нуево-Леон, Центр досліджень фізико-математичних наук, факультет фізико-математичних наук Авеню Педро де Альба, Університетське місто, Сан-Ніколас-де-лос-Гарса, Нуево-Леон, 66455, Мексика*
*[b]Вищий інститут прикладних наук і технологій Гаванського університету, пр. Сальвадора Альенде 1110 CP 10400, Гавана, Куба*
*[c]Фізичний центр, Венесуельський інститут наукових досліджень – IVIC, 20632, Каракас 1020-A, Венесуела*

У цій роботі досліджувалися структурні, морфологічні та оптичні властивості тонких плівок алюмінію (Al) та оксиду алюмінію ($Al_2O_3$), нанесених методом радіочастотного (РЧ) магнетронного розпилення. Плівки вирощували з використанням високочистої мішені з Al у контрольованих атмосферах, що містили різні потоки аргону (Ar) та кисню ($O_2$). Особливу увагу приділяли тому, як відстань між мішенню та підкладкою та співвідношення потоків Ar/$O_2$ впливають на структурні властивості плівок, особливості поверхні та оптичну реакцію. Методи характеристики включали рентгенівську дифракцію (XRD) для ідентифікації фаз та оцінки розміру кристалітів, атомно-силову мікроскопію (АСМ) для аналізу морфології та шорсткості поверхні, а також УФ-спектроскопію для вимірювання оптичного пропускання. Результати показали, що зменшення відстані між мішенню та підкладкою призводить до отримання плівок зі збільшенням шорсткості поверхні, товщини, розміру зерен та розміру кристалітів, ймовірно, через посилене енергетичне бомбардування та рухливість адатомів. Оптичні вимірювання показали, що плівки $Al_2O_3$, вирощені при вищих швидкостях потоку $O_2$ (близько 5 куб. см³/см³), були дуже прозорими, демонструючи значення пропускання близькі до 100% у всьому УФ-видимому діапазоні (190-900 нм). На противагу цьому, плівки, осаджені в умовах низького потоку $O_2$ (0,6-1,4 куб. см³/см³), були майже непрозорими, що свідчить про неповне окислення або металеву поведінку. Рентгенівський дифракційний аналіз показав, що вищі потоки $O_2$ мали тенденцію пригнічувати кристалічність, що призводило до аморфних плівок $Al_2O_3$, тоді як нижчі потоки зберігали певний ступінь кристалічного порядку. Крім того, збільшення швидкості потоку Ar під час осадження сприяло росту плівок, про що свідчить збільшення товщини плівки, що може бути пов'язано з підвищеною ефективністю розпилення та потоком атомів мішені. Ці результати підкреслюють критичну роль параметрів осадження у визначенні властивостей тонких плівок на основі Al для оптичних та електронних застосувань.

**Ключові слова:** *алюміній; тонкі плівки; магнетронне розпилення; відстань між мішенню та підкладкою; швидкість потоку Ar*